Published in final edited form as:

Cell Rep. 2019 May 14; 27(7): 2063–2074.e5. doi:10.1016/j.celrep.2019.04.022.

Acetate Promotes T Cell Effector Function during Glucose Restriction

Jing Qiu[1,8], **Matteo Villa**[1,8], **David E. Sanin**[1], **Michael D. Buck**[1], **David O'Sullivan**[1], **Reagan Ching**[1], **Mai Matsushita**[1], **Katarzyna M. Grzes**[1], **Frances Winkler**[7], **Chih-Hao Chang**[2], **Jonathan D. Curtis**[1], **Ryan L. Kyle**[1], **Nikki Van Teijlingen Bakker**[1], **Mauro Corrado**[1], **Fabian Haessler**[1], **Francesca Alfei**[3], **Joy Edwards-Hicks**[1], **Leonard B. Maggi Jr.**[4], **Dietmar Zehn**[3], **Takeshi Egawa**[5], **Bertram Bengsch**[6], **Ramon I. Klein Geltink**[1], **Thomas Jenuwein**[1], **Edward J. Pearce**[1,7], and **Erika L. Pearce**[1,9,*]

[1]Max Planck Institute of Immunobiology and Epigenetics, Freiburg 79108, Germany

[2]The Jackson Laboratory, Bar Harbor, ME 04609, USA

[3]School of Life Science, Technical University of Munich, 80333 Munich, Germany

[4]ICCE Institute and Department of Medicine, Division of Molecular Oncology, Siteman Cancer Center, Washington University School of Medicine, St. Louis, MO 63110, USA

[5]Department of Pathology and Immunology, Washington University School of Medicine, St. Louis, MO 63110, USA

[6]BIOSS Center for Biological Signaling Studies, University of Freiburg, 79104 Freiburg, Germany

[7]Faculty of Biology, University of Freiburg, 79104 Freiburg, Germany

[8]These authors contributed equally

[9]Lead Contact

SUMMARY

Competition for nutrients like glucose can metabolically restrict T cells and contribute to their hyporesponsiveness during cancer. Metabolic adaptation to the surrounding microenvironment is therefore key for maintaining appropriate cell function. For instance, cancer cells use acetate as a substrate alternative to glucose to fuel metabolism and growth. Here, we show that acetate rescues effector function in glucose-restricted $CD8^+$ T cells. Mechanistically, acetate promotes histone acetylation and chromatin accessibility and enhances IFN-γ gene transcription and cytokine production in an acetyl-CoA synthetase (ACSS)-dependent manner. *Ex vivo* acetate treatment

*Correspondence: pearce@ie-freiburg.mpg.de.

AUTHOR CONTRIBUTIONS

J.Q., M.V., D.E.S., M.D.B., D.O., R.C., C.-H.C., F.W., and E.L.P. designed, performed, and analyzed experiments. M.M., K.M.G., R.I.K.G., C.-H.C., J.D.C., R.L.K., N.V.T.B., M.C., F.H., F.A., and J.E.-H. provided technical assistance and critical expertise. L.B.M., D.Z., T.E., B.B., T.J., E.J.P., and E.L.P. provided reagents and conceptual input. J.Q., M.V., and E.L.P. wrote the manuscript.

SUPPLEMENTAL INFORMATION

Supplemental Information can be found online at https://doi.org/10.1016/j.celrep.2019.04.022.

DECLARATION OF INTERESTS

E.J.P. is a founder of Rheos Medicines and E.L.P. is an SAB member of ImmunoMet and a founder of Rheos Medicines.

increases IFN-γ production by exhausted T cells, whereas reducing ACSS expression in T cells impairs IFN-γ production by tumor-infiltrating lymphocytes and tumor clearance. Thus, hyporesponsive T cells can be epigenetically remodeled and reactivated by acetate, suggesting that pathways regulating the use of substrates alternative to glucose could be therapeutically targeted to promote T cell function during cancer.

In Brief

Qiu et al. show that acetate enhances histone acetylation, chromatin accessibility, and effector function in glucose-restricted $CD8^+$ T cells. The authors find that manipulation of acetate-handling pathways influences cytokine production of tumor-infiltrating $CD8^+$T cells, which could have therapeutic implications for activating $CD8^+$ T cell effector function in the tumor microenvironment.

Graphical Abstract

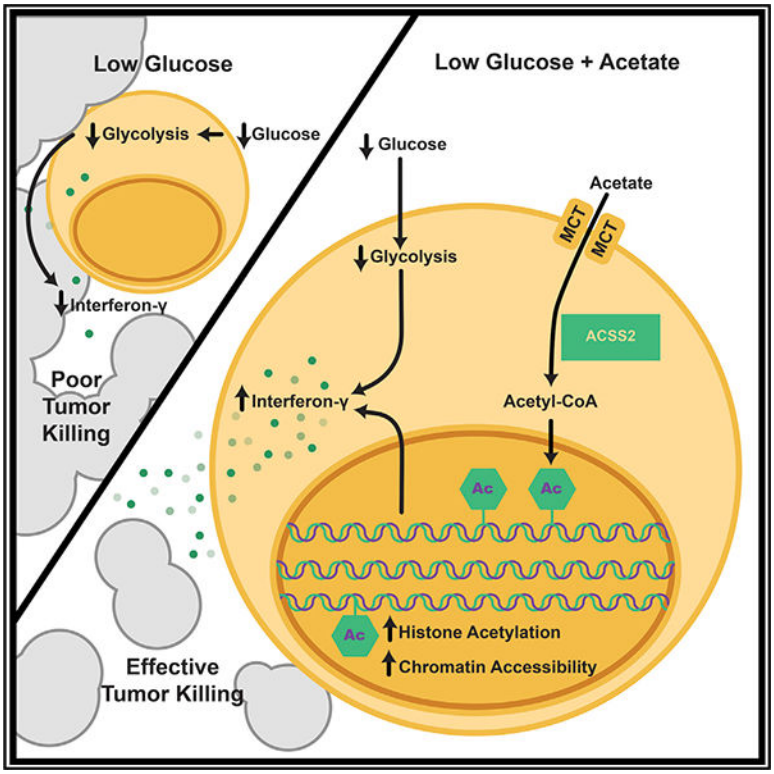

INTRODUCTION

Metabolic fitness is important for proper T cell function. Upon activation, T cells require increased glucose uptake to meet the energy and biosynthesis demands required for T cell activation, clonal expansion, and effector function (Pearce and Pearce, 2013; Pearce et al., 2013). Many observations collectively support the importance of glucose for T cell responses. Culturing T cells in limited glucose inhibits the proliferation, survival, and expression of effector molecules, including interferon-g (IFN-γ) (Cham et al., 2008; Cham

and Gajewski, 2005; MacIver et al., 2013). Similarly, surface expression of the glucose transporter Glut-1 is critical during activation to sustain T cell effector function (Jacobs et al., 2008). Glycolysis promotes IFN-γ expression both through epigenetic and post-transcriptional mechanisms (Chang et al., 2013; Peng et al., 2016), whereas glycolysis inhibition leads to increased expression of immune-regulatory receptors, such as programmed cell death protein-1 (PD-1), which can drive T cell exhaustion (Bengsch et al., 2016; Patsoukis et al., 2015).

Further *in vivo* models support the importance of glucose availability to sustain T cell function. T cells isolated from fasting animals exhibit long-lasting metabolic and functional defects marked by decreased glucose uptake (Saucillo et al., 2014). Also, T cells in the tumor microenvironment must compete with tumor cells for available glucose, which limits T cell activity and favors tumor progression (Chang et al., 2015; Ho et al., 2015). Effector T cells and tumor cells share many metabolic features, such as engaging Warburg metabolism (aerobic glycolysis) or exhibiting increased dependence on glutamine to support biosynthesis needs. Tumor cells and immune cells also compete for other nutrients, such as the amino acids tryptophan and argi-nine (Renner et al., 2017).

It is well recognized that the short-chain fatty acid acetate is an important alternative carbon source for cancer cells to support survival and proliferation under low-glucose conditions (Bulusu et al., 2017; Comerford et al., 2014; Lyssiotis and Cantley, 2014; Schug et al., 2015). Acetate also has a major effect on immune cell function. For example, a systemic increase in acetate induced by infection is required for optimal memory $CD8^+$ T cell function via a mechanism involving increased GAPDH acetylation and enhanced glycolysis (Balmer et al., 2016). Furthermore, addition of acetate *in vitro* has been shown to enhance IFN-γ gene transcription (Peng et al., 2016). Further stressing the role of acetate in enhancing the immune response, synthesis of acetate from ethanol is critical for enhancing the inflammatory response in macrophages through increased histone acetylation at promoter regions of pro-inflammatory genes in acute alcoholic hepatitis (Kendrick et al., 2010). Given the potential competition between tumor cells and effector T cells to access glucose, we set out to explore whether acetate could correct cytokine production in glucose-restricted T cells and, ultimately, T cells in the tumor microenvironment.

RESULTS

Acetate Restores IFN-γ Production in T Cells under Chronic Glucose Restriction

To understand how T cells metabolically adapt to nutrient-restrictive environments, we established an *in vitro* model in which naive OT-I T cells were activated with ovalbumin (OVA) peptide in medium containing 25 mM glucose and then cultured in medium containing 1 mM glucose for 1 or 5 days, followed by overnight culture supplemented with or without 5 mM acetate (Figure 1A). To examine how acetate affects T cell responsiveness in low glucose, we measured intracellular IFN-γ after phorbol 12-myristate 13-acetate (PMA)-ionomycin restimulation. As expected, T cells cultured in 1 mM glucose produced significantly less IFN-γ compared with T cells cultured in 25 mM glucose (Figures S1A and S1B). However, IFN-γ expression was markedly increased in cells that had been supplemented with 5 mM acetate compared with those in 1 mM glucose alone (Figures 1B

and 1C). These effects were accompanied by an associated increase in *Ifng* mRNA after acetate treatment (Figure 1D). Acetate also significantly boosted IFN-γ secretion by cells from the day 9 time point, suggesting that the effect of acetate intensifies over prolonged glucose restriction (Figure 1E). Importantly, supplemental acetate did not affect cell survival (Figure 1F), proliferation (Figure 1G), or lactate secretion (Figure 1H), which was instead decreased in cells cultured in 1 mM glucose compared with cells cultured in 25 mM glucose (Figure S1C). These data indicate that, although acetate substituted for glucose in terms of restoring cytokine production, it did not substitute for glucose in other metabolic processes in the cell. Furthermore, supplemental acetate had little effect on $CD8^+$ T cell activation marker expression (Figure S1D), cell size (Figure S1E), and granzyme B expression (Figure S1F).

Based on earlier work (Kendrick et al., 2010), we reasoned that the increased IFN-γ mRNA (Figure 1D) could reflect the ability of acetate to substitute for glucose-derived citrate in the production of acetyl-CoA, which serves as an acetyl donor for histone acetylation and, therefore, supports gene transcription. Consistent with this idea, we observed enhanced IFN-γ protein and *Ifng* mRNA expression in T cells exposed to valproic acid (VPA), a histone deacetylase inhibitor that augments global histone acetylation (Göttlicher et al., 2001) (Figures 1B–1D). These results illustrate that increased histone acetylation correlates with enhanced T cell effector function, even in T cells exposed to low-glucose conditions (Agarwal et al., 2009; Araki et al., 2008).

Acetate Is Incorporated into Histones and Enhances Histone Acetylation in Glucose-Restricted T Cells

To determine whether acetate enhances IFN-γ production in glucose-deprived T cells by promoting histone acetylation and supporting gene transcription, we first asked whether glucose-restricted T cells are able to competently acquire and utilize exogenous acetate. Acetate enters cells through monocarboxy-late transporters (MCTs) or aquaporins (Halestrap and Wilson, 2012; Kirat and Kato, 2006; Kirat et al., 2006; Rae et al., 2012) and, when in the cell, can be converted to acetyl-coenzyme A (CoA) (Watkins et al., 2007) by one of three acetyl-CoA synthetase enzymes (ACSS1–ACSS3). Acetyl-CoA is essential for many biological processes, including protein acetylation and lipogenesis. Because MCT-1 and MCT-4 have been reported to mediate significant transport of acetate in many tissues (Merezhinskaya et al., 2004), we questioned whether glucose-restricted T cells were competent in importing exogenous acetate. We observed that MCT-1 and MCT-4 proteins were expressed on T cells over a range of glucose concentrations (Figures S2A and S2B). Moreover, their expression was stable throughout the duration of the culture, supporting the notion that T cells could acquire acetate when available in the extracellular environment. We also found that ACSS2, the isoform that plays the dominant role in acetate utilization in mammalian cells (Comerford et al., 2014), was expressed in T cells and was unaffected by glucose concentration (Figure S2A).

To assess whether T cells acquired exogenous acetate, we exposed activated T cells to radioactive [1,2-^{14}C] acetate and measured the incorporation of ^{14}C into histones and lipids. ^{14}C was enriched in both histones (Figure 2A) and lipids (Figure S2C). We next assessed

global histone acetylation in glucose-restricted T cells by western blotting. We found that acetylation of the his-tone proteins H3 and H4 was increased by supplemental acetate (Figure 2B). We also observed that T cells under prolonged glucose restriction (day 9) had lower H3K9–14 and H3K27 acetylation compared with cells under acute glucose restriction (day 5), and these acetylation marks were restored by addition of acetate (Figures 2C and S2D). Of note, VPA treatment increased histone acetylation at all time points (Figures 2B and 2C).

We further assessed the effects of supplemental acetate on histone acetylation by performing genome-wide ChIP sequencing analysis of acetylation of H3K27 in T cells cultured in 1 mM glucose with or without supplemental acetate. We found that acetate supplementation modestly increased H3K27 acetylation in an area of 2 kbp around the transcription start sites (TSSs) of genes in clusters 1, 2, and 3, where clusters are defined by their similarity in H3K27 acetylation profile (Figures 2D and 2E); no substantial H3K27 acetylation was detected around the TSSs of genes in cluster 4. This analysis also revealed that there was no marked difference in the pattern of H3K27 acetylation around TSSs but, rather, that acetate supplementation globally enriches the overall level of acetylation (Figure 2E). These findings are in keeping with our hypothesis that glucose-restricted T cells are able to acquire and utilize acetate to promote histone acetylation.

Acetate Promotes Chromatin Accessibility in Glucose-Restricted T Cells

The increased histone acetylation, a process known to correlate with transcriptional activation (Allfrey et al., 1964; Verdin and Ott, 2015), evident in glucose-restricted T cells after supplemental acetate prompted us to perform ATAC-seq analysis. We expected these data to reveal whether the enhanced histone acetylation evident after acetate treatment was linked to changes in chromatin accessibility. We compared the chromatin profiles of T cells cultured in 1 mM glucose with or without supplemental acetate from different time points (day 5 and 9). We found that day 5-activated T cells cultured in 1 mM glucose with acetate had increased chromatin accessibility at 41 regions (Figure 3A) compared with cells cultured in 1 mM glucose alone. Cells that were cultured for an additional 4 days in 1 mM glucose (day 9) and then treated with acetate showed increased accessibility at 255 regions (Figure 3B) compared with cells cultured in 1 mM glucose alone. Together, our data show that acetate promotes histone acetylation and chromatin accessibility in T cells that are under glucose-limiting conditions and that this effect of acetate intensifies the longer the cells are deprived of glucose.

We also performed a pathway analysis of the 263 genes marked by peaks after acetate treatment on day 9 and found that the majority of significant gene ontology terms were related to signaling pathways (Tables S1A and S1B). Of note, one of these genes was *Bhlhe40*, which is a transcription factor that is critical for T cell function (Lin et al., 2014) and for maintaining active histone marks at the loci of $CD8^+$ T cell effector molecules (Li et al., 2018, J. Immunol., abstract). Overall, the data suggest that, in the face of glucose restriction, supplemental acetate facilitates chromatin accessibility at genes that promote $CD8^+$ T cell effector function.

Acetate Augments Expression of a Cohort of Restimulation-Associated Genes in Glucose-Restricted T Cells

To assess whether acetate treatment increases effector gene expression in T cells experiencing glucose restriction, we performed RNA sequencing (RNA-seq) analysis on T cells after PMA-ionomycin restimulation. Principal-component analysis revealed that the most significant changes in gene expression correlated to the length of time in culture, whereas, by comparison, acetate supplementation had a limited effect on the transcriptional profiles (Figure 3C). Focusing on analysis of different time points, we found that acetate supplementation substantially affected the transcriptional landscape of cells cultured in 1 mM glucose, with 1,109 differentially expressed genes (DEGs) on day 5 and 461 DEGs on day 9, between the conditions (Figure 3D). A cohort of 151 DEGs was commonly regulated by acetate at both time points (Figure 3D). To assess whether acetate had any transcriptional effect on effector T cell function, we performed a gene ontology analysis of the DEGs identified in Figure 3D and concentrated on the top 5 enriched pathways in each group (Figure 3E). We identified a cohort of restimulation-associated genes belonging to immune response-related pathways whose expression was enhanced by acetate. Among those, we found genes encoding for IFN-γ, granzymes, tumor necrosis factor (TNF), and the transcription factor T-bet (*Tbx21*), which controls IFN-γ expression (Szabo et al., 2000; Figure 3E). Of note, acetate increased the expression of some of these transcripts, such as *Tnf* and *Tbx21*, only at day 9, suggesting that acetate can have additional effects on T cell effector function after prolonged glucose restriction.

Ex Vivo Acetate Treatment Enhances IFN-γ Production in Exhausted T Cells

Our *in vitro* culture model allowed us to tightly control glucose availability. However, we next aimed to obtain more direct *in vivo* evidence to support our findings. To this end, we isolated tumor-infiltrating lymphocytes (TILs) from B16 melanoma tumors 21 days after subcutaneous implantation in mice (Figure 4A) and treated them with or without supplemental acetate *ex vivo*. Based on earlier work (Chang et al., 2015; Ho et al., 2015), we reasoned that, at this later time point, TILs would have experienced prolonged glucose restriction and shown some hyporesponsive phenotypes analogous to T cells cultured in 1 mM glucose. Indeed, as in T cells cultured under glucose restriction (data not shown), PD-1 was highly expressed on the isolated TILs (Figure 4B). Moreover, treating TILs for 4 h with supplemental acetate *ex vivo* significantly increased the fraction of TILs expressing IFN-γ after PMA-ionomycin restimulation compared with PBS-treated TILs (Figures 4C–4E), indicating that acetate promotes responsiveness in T cells isolated directly from the tumor microenvironment. We also co-transferred OT-I $CD8^+$ T cells and EL4-OVA lymphoma tumor cells into mice and, 6 days later, administered one intraperitoneal injection of acetate (500 mg/kg) (Figure 4F). Upon SIINFEKL peptide restimulation, we found that acetate administration significantly increased the frequency of IFN-γ-producing donor cells isolated from the peritoneal cavity compared with PBS-injected controls (Figures 4G–4I).

To further corroborate our findings, we isolated lymphocytes from the blood of patients chronically infected with hepatitis C virus (HCV). We hypothesized that, in this scenario, T cells may experience a setting that is similar to glucose restriction, whether from a lack of available substrate or a lack of ability to acquire substrate, during their response to persistent

virus infection that may potentially lead to T cell exhaustion and/or hyporesponsiveness (Bengsch et al., 2016; Wedemeyer et al., 2002). We found that acetate treatment increased the expression of effector cytokines such as IFN-γ and TNF only in $CD8^+$ T cells expressing high levels of PD-1 compared with PBS-treated counterparts (Figure 4J and 4K). Of note, acetate also enhanced the expression of XCL-1 while not affecting CCL-3 and interleukin-2 (IL-2) expression (Figures S3A–S3C). Taken together, our data show that exogenous acetate increases histone acetylation, chromatin accessibility, and cytokine production even in cells under prolonged glucose restriction.

The Enhancing Effect of Acetate on IFN-γ Production Is Dependent on ACSS Enzymes

We reasoned that acetate was able to restore the function of glucose-restricted T cells by providing cells with an alternative substrate for dynamic histone acetylation required for activation-induced gene expression. This process would require the ACSS-mediated conversion of cytosolic acetate to acetyl-CoA (Bulusu et al., 2017; Mews et al., 2017). We next tested whether the acetate-dependent rescue of cytokine production was dependent on ACSS2. We used short hairpin RNAs (shRNAs) to selectively silence *Acss2* (*Acss2* shRNA; Figure 5A). Suppression of ACSS2 by *Acss2* shRNA rendered glucose-restricted T cells less responsive to the acetate-driven increases in IFN-γ production (Figure 5B), an effect that was accompanied by reduced incorporation of ^{14}C carbon from radioactively labeled acetate into histones (Figure 5C). This did not reflect a histonespecific event because acetate-derived carbon incorporation into fatty acids was also diminished in *Acss2* shRNA-treated T cells (Figure 5D), presumably reflecting diminished overall availability of the acetyl-CoA donor. Together, these data support the view that, in glucose-restricted T cells, cytokine production can be promoted by exogenous acetate through ACSS2-dependent production of acetyl-CoA, which serves as a donor for histone acetylation, promoting activation-induced gene expression.

To validate our approach, we traced heavy labeled ^{13}C-acetate into tricarboxylic acid (TCA) cycle intermediates using mass spectrometry in T cells transduced with *Acss1/2* shRNA and observed decreased ^{13}C incorporation into fatty acids and TCA cycle intermediates (Figure 5E). Enforced expression of *Acss2* in T cells increased ^{13}C-acetate-derived carbon incorporation in citrate and fatty acids (Figure 5F). Together, these data indicate that ACSS enzymes mediate the conversion of exogenously supplied acetate to acetyl-CoA, which then feeds into different metabolic pathways.

ACSS2 Expression Contributes to Optimal Effector T Cell Function *In Vivo*

To circumvent possible confounding issues of adding exogenous acetate to cultured cells, we assessed the role of ACSS2 on IFN-γ production by T cells in an *in vivo* setting. We remained focused on ACCS2 because this isoform was expressed by $CD8^+$ T cells (Figure S2A), was shown to be critical for acetate utilization (Comerford et al., 2014), and because of our *Acss2* shRNA data (Figures 5A–5F). We subcutaneously injected 1×10^6 EL4-OVA lymphoma tumor cells and then intravenously transferred 5×10^6 activated OVA-specific OT-I cells transduced with either control or *Acss2* shRNA into $Thy1.1^+$ recipient mice 5 days post-tumor transplantation (Figure 5G). On day 7, we examined donor OT-I T cells in the peripheral blood and found that *Acss2* knockdown significantly reduced the fraction of

cells capable of producing IFN-γ and negatively affected the amount of IFN-γ produced by the cells (Figures 5H–5J). Consistent with these findings, tumor clearance was impaired in mice that received *Acss2* shRNA-transduced OT-I T cells compared with those that received OT-I T cells transduced with the control shRNA (Figure 5K). Further analysis revealed that TILs expressing *Acss2* shRNA exhibited reduced IFN-γ expression compared with TILs expressing control shRNA (Figures 5G and 5L–5N). These data suggest that antigen-specific T cell effector functions are supported by ACSS2 under nutrient-limiting conditions such as cancer, presumably by permitting T cells to utilize endogenous acetate.

DISCUSSION

T cells must acquire sufficient nutrients to engage the appropriate metabolism to support effector functions during infection and cancer (Buck et al., 2015, 2017; Buck et al., 2017; Chang et al., 2013; Michalek and Rathmell, 2010; O'Sullivan and Pearce, 2015; Pearce et al., 2013). Nutrient competition can remarkably influence the immune response, and nutrient depletion in the tumor microenvironment can lead to T cell hyporesponsiveness and tumor progression (Chang et al., 2015; Ho et al., 2015; Mellor and Munn, 2008; Mockler et al., 2014). A recent paper showed that TILs in renal cell carcinoma suffer from glycolytic and mitochondrial insufficiency, which impairs their function (Siska et al., 2017), further highlighting the importance of appropriate metabolic remodeling in these cells.

As a primary energy resource, glucose plays an essential role in supporting cellular bioenergetics and maintaining normal cell function. When transiting to environments with limited nutrients and oxygen, cancer cells reprogram their metabolism to cope with environmental changes in a manner dependent on alterative substrates, as do immune cells. We found that acetate, a unique metabolite positioned at the intersection of metabolism and epigenetic regulation, enhances IFN-γ production from T cells during prolonged glucose restriction. The maintenance of MCT-1, MCT-4, and ACSS2 expression over a range of glucose concentrations indicates that T cells maintain the ability to acquire and utilize acetate in situations when glucose becomes limited. Although acetate was able to restore cytokine production in these cells, and it contributed to histone acetylation, it did not replace the effects of glucose in terms of lactate production and proliferation. Acetate feeds into the cellular pool of acetyl-CoA and takes part in the TCA cycle and in subsequent anabolic pathways, such as fatty acid, cholesterol, and hexosamine biosynthesis (Puleston et al., 2017). It is possible that acetate does not substitute for glucose in the glycolysis pathway and in those branching from it, such as the pentose phosphate and serine biosynthesis pathways, which are key to sustaining T cell proliferation (Ma et al., 2017).

Our data highlight the role of acetate as an alternative carbon source for histone acetylation in T cells when access to glucose is limited. Although our studies did not investigate ACSS localization, it is possible that the observed enhancement in T cell cytokine production after acetate treatment is the result of differential expression of ACSS2 in the nuclear compartment, which has been shown to directly maintain histone acetylation in cancer cells and neurons (Bulusu et al., 2017; Mews et al., 2017). In our *in vitro* culture system, we used 5 mM sodium acetate, which may be considered a non-physiological concentration because acetate levels in healthy human and murine blood range from 50 to 600 mM (Hosios and

Vander Heiden, 2014). However, during infection, serum acetate concentrations in mice have been shown to reach 2–5 mM (Balmer et al., 2016). Also, chronic alcoholics have blood acetate levels in the range of 1 mM, indicating that blood acetate levels can be much higher depending on the context (Nuutinen et al., 1985). It is also interesting to consider that acetate levels in local microenvironments and particular niches may be higher than what is measured in the blood. A recent study has revealed that diet-derived short-chain fatty acids (SCFAs), including acetate, boost $CD8^+$ T cell effector function by enhancing cellular metabolism (Trompette et al., 2018). More work will need to be done to determine the relevance of acetate utilization by T cells in a variety of *in vivo* settings.

Our data showed that supplemental acetate enhances global acetylation of histones and that 263 genes had enhanced accessibility after acetate treatment (Table S1A), and within these peaks were genes, such as *Bhlhe40*, with important roles in T cell function (Lin et al., 2014; Li et al., 2018, J. Immunol., abstract). Acetate exposure also slightly increased accessibility to the promoter region of T-bet (encoded by the gene *Tbx21*), which may correlate with the increased T-bet gene expression evident after acetate treatment (Figure 3E). Of note, the IFN-γ gene was equally accessible in acetate-treated and -untreated cells. This suggested to us that mechanisms in addition to chromatin accessibility, such as transcription factor binding driving gene expression, contribute to differences in IFN-γ production upon acetate exposure. Overall, our data imply that, within the genes represented by the open chromatin peaks, there are genes that encode proteins that regulate the expression of the 461 DEGs emerging from the RNA-seq data of day 9 acetate-treated cells. Although not addressed in this study, the relationship between genes in open chromatin and DEGs as well as how these DEGs regulate T cell function are subjects of future investigation.

In summary, we have shown that prolonged glucose restriction contributes to T cell hyporesponsiveness characterized by defects in IFN-γ production and that administration of acetate promotes chromatin accessibility, histone acetylation, and cytokine production in glucose-restricted T cells in an ACSS-dependent manner. Recent studies have shown that exhausted T cells have progressively acquired, exhaustion-associated DNA methylation programs (Pauken et al., 2016) and that blocking this epigenetic reprogramming may boost immune checkpoint blockade therapies (Ghoneim et al., 2017). The SCFA acetate can promote chromatin accessibility, histone acetylation, and IFN-γ production in T cells rendered hyporesponsive by glucose restriction. Understanding nutrient competition in the tumor microenvironment and how this affects T cell nutrient acquisition may be an important component in the generation of future therapies to promote durable T cell immunity in cancer.

STAR★METHODS

CONTACT FOR REAGENT AND RESOURCE SHARING

Further information and requests for resources and reagents should be directed to and will be made available upon reasonable request by the Lead Contact, Erika L. Pearce (pearce@ie-freiburg.mpg.de).

EXPERIMENTAL MODEL AND SUBJECT DETAILS

Mice and tumor models—OT-I transgenic mice (C57BL/6-Tg(TcraTcrb)1100Mjb/J; Jax, 003831), CD45.1$^+$ C57BL/6J (B6.SJL-*Ptprc*^{a} *Pepc*^{b}/BoyJ; Jax, 002014), Thy1.1$^+$ C57BL/6J (B6.PL-*Thy1*^{a}/CyJ; Jax, 000406) and C57BL/6J (Jax, 000664) mice were purchased from the Jackson Laboratory and were housed under specific pathogen-free conditions at the Max Planck Institute of Immunobiology and Epigenetics or at Washington University School of Medicine, according to the Institutional Animal Use and Care Guidelines. Experimental procedures have been authorized by animal welfare committees at the Washington University School of Medicine or at the Max Planck Institute of Immunobiology and Epigenetics. All procedures have been carried out following Institutional Animal Use and Care Guidelines in compliance with US, or German and European regulations.

Adult mice (older than 8 weeks old) of both sexes were used in the experiments reported in the manuscript. Comparisons were performed between sex- and age-matched mice.

For the experiments in Figures 4A–4E, the flanks of CD45.1$^+$ C57BL/6 mice were shaved and the mice were subcutaneously injected with 10^6 B16 melanoma tumor cells in 100 μL PBS. Tumor growth was monitored every 2–3 days by measuring the diameter of the tumor mass. On day 21 after tumor implant, mice were humanely euthanized and the tumor mass harvested and further processed (see below). For the experiments in Figures 4F–4I, 10^7 EL4-OVA lymphoma tumor cells were intraperitoneally injected in 200 μL of PBS in CD45.1$^+$ C57BL/6 mice. Concomitantly, 2×10^4 naive OT-I CD8$^+$ T cells were intravenously injected in the same mice. 6 days after the tumor transfer, mice were treated with either a single bolus of sodium acetate in PBS (500 mg/Kg) or with PBS alone. 1 day later, mice were euthanized and the peritoneal content was harvested for further analysis. For experiments in Figures 5G–5N, the flanks of Thy1.1$^+$ C57BL/6 mice were shaved and the mice were subcutaneously injected with 10^6 EL4-OVA lymphoma tumor cells in 100 μL PBS. 5 days later, mice received 5×10^6 activated OT-I cells transduced with the viruses indicated in the text. On day 7, mice were bled and the cells processed for further analysis. Tumor growth was monitored every 2–3 days by measuring the diameter of the tumor mass.

Human blood analysis—Human samples were obtained according to German federal guidelines, local ethics committee regulations (Albert-Ludwigs-University, Freiburg, Germany, HBUF 474/14 and 243/18) and the Declaration of Helsinki (1975). 8/9 blood samples were obtained from male individuals, between 46 and 72 years old. 1/9 blood sample was obtained from a female individual, 56 years old.

Blood samples from patients chronically infected with HCV were processed to isolated PBMCs that were then stored at 80 C until analysis. PBMCs were treated overnight with 5 mM sodium acetate or PBS, in medium containing FBS. Cells were then restimulated with PMA/Ionomycin and brefeldin A for 4 hours before processing them for surface and intracellular staining.

Cell culture—OVA peptide-specific T cells were isolated from spleens and peripheral lymph nodes of OT-I transgenic mice (older than 8 weeks old, sex- and age-matched) and activated with the ovalbumin peptide SIINFEKL ($OVA_{257–264}$, 100 ng/ml, New England

Peptide). T cells were cultured in RPMI 1640, added with 10% heat-inactivated fetal bovine serum (GIBCO, lot n. 1640960), glutamine (4 mM), penicillin/streptomycin (1%), b-mercaptoethanol (55 μM) and glucose (concentrations indicated in the text). Cells were grown at 37°C, in 5% CO_2, atmospheric O_2, in a humidified incubator. Briefly, cells were activated on day 0 with $OVA_{257–264}$, with rhIL-2 (100 U/ml, Peprotech) in medium containing 25 mM glucose. After 3 days, cells were either kept in 25 mM glucose or switched to 1 mM glucose for 1 or 5 days. 1 day before analysis, cells maintained in 1 mM glucose were treated with or without 5 mM sodium acetate (Sigma) or valproic acid (1 mM, Sigma). Starting from day 2, and every day, cultured cells were harvested, washed, counted and plated at a concentration of 10^6 cells/ml in fresh medium with rhIL-2.

B16 melanoma tumor cells (kindly provided by Dr. Marco Colonna) and EL4-OVA lymphoma tumor cells (E.G7-OVA [derivative of EL4]; ATCC, CRL-2113) were cultured in the medium described above, with addition of 10 mM glucose, and in the culture conditions previously described. Additional information regarding the sex of the cell lines could not be found on the ATCC website.

METHOD DETAILS

Tumor processing—Solid tumors (Figures 4A–4E and 5G–5N) were excised from mice at the indicated time post-implant and kept at +4°C. Isolated tumors were finely chopped and treated with type IA collagenase (Sigma, 1 mg/ml) and DNase I (Sigma, 50 μg/ml) in Hanks' Balanced Salt Solution (HBSS, Hyclone) for 1 hour at 37°C. After digestion, cells were washed and filtered through a 70 μm strainer to obtain single cell suspensions.

Retroviral transduction—OT-I $CD8^+$ T cells were activated with $OVA_{257–264}$ and rhIL-2 (100 U/ml) for 27 hours in the previously described medium added with 10 mM glucose. Cells were then transduced with viruses expressing short hairpin RNA (hp) against luciferase (Ctrl Hp -GFP-), *Acss2* (*Acss2* Hp -GFP-), *Acss1* (*Acss1* Hp -hCD8-) or with the expression constructs (Ctrl OE or *Acss2* OE -both expressing GFP-). Transduction was performed in the previously described medium added with polybrene (Sigma, 8 μg/ml), HEPES (Hyclone, 10 mM), gluta-mine (4 mM) and rhIL-2 (100 U/ml). Cells were centrifuged at 2500 rpm, for 90 minutes at 30°C, followed by 3 hours resting in the same medium. Transduced cells were then used for further analysis.

Flow cytometry—The following antibodies were used to perform surface and intracellular staining: anti-CD8α (53–6.7, Biolegend); anti-CD44 (IM7, Biolegend); anti-CD45.1 (A20, Biolegend); anti-CD45.2 (104, Biolegend); anti-PD-1 (J43, Invitrogen); anti-CD25 (3C7, Biolegend); anti-CD69 (H1.2F3, Biolegend); anti-CD62L (MEL-14, Biolegend); anti-CD71 (RI7217, Biolegend); anti-Granzyme B (NGZB, eBioscience); anti-IFNγ (XMG1.2, Biolegend); anti-GFP (FM264G, Biolegend). Live cell were identified using the LIVE/DEAD fixable dead cell stain from Invitrogen.

Surface staining was performed in PBS containing 2% FBS and EDTA (2 mM), on ice for 30 minutes. Cytokine production was analyzed by intracellular staining upon restimulation with phorbol 12-myristate 13-acetate (PMA, Sigma, 50 ng/ml)/ionomycin (Sigma, 500 ng/ml) in presence of brefeldin A (Biolegend, 0.1%) for 4 hours, or with SIINFEKL peptide

(100 ng/ml) in presence of brefeldin A for 12 hours. After stimulation, cells underwent surface staining, followed by fixation in Cytofix/Cytoperm fixation buffer (BD Biosciences) at +4°C for 15 minutes. Cells were then thoroughly washed, antibodies against intracellular antigens were added in presence of 1X permeabilization buffer (BD Biosciences) and the suspension was incubated for 45 minutes, on ice in the dark. CellTrace Violet (CTV) reagent (Invitrogen) was used to assess cell proliferation following the manufacturer recommendations. Cell proliferation was measured based on the fraction of live cells that diluted CTV over a period of 24 hours. Samples were assessed with FACSCalibur, FACSCanto II or LSRFortessa analyzers (BD Biosciences), or sorted using FACSAria cell sorters. Acquisition data were analyzed with FlowJo software (TreeStar).

Lactate measurement—Production of lactate, as a measure of aerobic glycolysis, was quantified in the supernatant of cultured cells 24 hours after seeding 10^6 cells/mL. Quantification was performed using a Roche Cedex Bio analyzer following manufacturer recommendations.

ELISA

Quantification of secreted IFN-g was assessed by ELISA (RND Systems) following manufacturer recommendations. Supernatant was collected 4 hours after PMA/Ionomycin restimulation of 10^6 cells/mL.

Metabolomic analysis—Upon retroviral transduction, GFP^+ cells were sorted by flow cytometry. Cells were then cultured in the above described medium containing 10 mM glucose, in presence of 5 mM of uniformly-labeled ^{13}C acetate, for 24 hours. Cells were washed with 0.9% NaCl and kept on ice. Intracellular metabolite extraction was performed with 70% ethanol, previously warmed up to 70°C. Samples were centrifuged, and the supernatants collected and dried under vacuum. Dried pellets were further processed and analyzed using gas chromatography-mass spectrometry (Agilent).

Real time quantitative PCR—RNA was extracted using RNAsolv reagent (Omega) according to manufacturer instructions. RNA to cDNA conversion was performed using the High Capacity cDNA Reverse Transcription Kit (Applied Biosystems). Quantification of target genes was done by quantitative PCR using Taqman technology (Applied Biosystems). Reaction mixes were run on the QuantStudio 3 Applied Biosystems thermal cycler. TaqMan primer pairs used to quantify target genes were as follow: *Ifng* Mm01168134_m1; *Hprt* Mm03024075_m1 (Applied Biosystems).

Western blotting—For western blot analysis cells were washed with ice cold PBS and lysed in lysis buffer (20 mM Tris-HCl, [pH 7.5], 150 mM NaCl, 1 mM Na_2EDTA, 1 mM EGTA, 1% Triton X-100, 2.5 mM sodium pyrophosphate, 1 mM b-glycerophosphate, 1 mM Na_3VO_4, 1 mg/mL leupeptin (Cell Signaling Technologies) supplemented with 1 mM PMSF. Samples were frozen and thawed 3 times followed by centrifugation at 20000 g for 10 min at +4°C. Cleared protein lysate was denatured with LDS loading buffer for 10 min at 70°C, and loaded on precast 4% to 12% bis-tris protein gels (Life Technologies). Proteins were transferred onto nitrocellulose membranes using the iBLOT 2 system (Life

Technologies) following the manufacturer's protocols. Membranes were blocked with 5% w/v milk and 0.1% Tween-20 in TBS and incubated with the appropriate antibodies in 5% w/v BSA in TBS with 0.1% Tween-20 overnight at 4°C. The following antibodies were used: anti-α-tubulin (Cell Signaling); anti-ACSS2 (Thermo Scientific); anti-MCT-4 (Santa Cruz); anti-MCT-1 (Santa Cruz); anti-H3 (Cell Signaling); anti-H4 (Cell Signaling); anti-Ac-H3 (Millipore); anti-Ac-H4 (Millipore); anti-Ac-H3K9/14 (Diagenode); anti-Ac-H3K27 (Diagenode). All primary antibody incubations were followed by incubation with secondary HRP-conjugated antibodies (Pierce) in 5% milk and 0.1% Tween-20 in TBS and visualized using SuperSignal West Pico Chemiluminescent Substrate (Pierce) on Biomax MR film (Kodak). Quantification of western blots was performed by densitometry using the ImageJ software (NIH). Arbitrary units (AU) were corrected for background signal and normalized to the loading control.

Analysis of ^{14}C acetate incorporation into histones—Cells were treated with 1 μCi/ml sodium [1,2-^{14}C] acetate (Perkin Elmer), overnight. After two washes in ice-cold PBS, cell pellets were re-suspended in 500 μL NP-40 buffer (0.1% NP-40, 10 mM HEPES, 5 mM $MgCl_2$, 0.25 M Sucrose) and incubated on ice for 10 minutes. Lysates were washed with the same buffer without NP-40 and spun down at 6000 g for 10 minutes. Histone were extracted in 500 μL of 0.8 M HCl, in shaking overnight and samples were then centrifuged at +4°C, 20.000 g for 30 minutes. Super-natants were neutralized with 40 μL of 10 N NaOH and radioactivity was calculated using Ultima Gold scintillation fluid.

Analysis of ^{14}C acetate incorporation into lipids—Cells were treated with 1 μCi/ml sodium [1,2-^{14}C] acetate (Perkin Elmer), overnight. After two washes in ice-cold PBS, cells were lysed with 0.6 mL of MeOH solution. 0.4 mL of $CHCl_3$ was added to lysate and vortexed for 30 s. Lysates were then centrifuged for 5 minutes at 1000 rpm for phase separation. Soluble lipid fraction was collected as the lower layer and radioactivity was counted using Ultima Gold scintillation fluid.

RNA sequencing analysis—RNA was extracted using the RNAsolv reagent (Omega) according to manufacturer instructions and quantified using Qubit 2.0 (Thermo Fisher Scientific) following the manufacturer's instructions. Libraries were prepared using the TruSeq stranded mRNA kit (Illumina) and sequenced in a HISeq 3000 (Illumina) by the Deep-sequencing Facility at the Max-Planck-Institute for Immunobiology and Epigenetics. Sequenced libraries were processed with the Galaxy platform and deepTools (Afgan et al., 2016; Ramírez et al., 2016), using STAR (Dobin et al., 2013), for trimming and mapping, and featureCounts (Liao et al., 2014) to quantify mapped reads. Raw mapped reads were processed in R (Lucent Technologies) with DESeq2 (Love et al., 2014), to determine differentially expressed genes and generate normalized read counts to visualize as heatmaps using Morpheus (Broad Institute). Gene ontology analysis was performed used the free online platform DAVID (Huang et al., 2009a, 2009b). RNA sequencing data are deposited in GEO under the following subseries code: GSE128591.

ATAC sequencing analysis—Libraries were prepared using the Nextera DNA library Prep Kit (Illumina) adapting a published protocol (Buenrostro et al., 2015). Briefly, 5×10^4 T

cells treated as described were washed in PBS and then lysed in 10 mM Tris-HCl, pH 7.4,10 mM NaCl, 3 mM $MgCl_2$ and 0.1% Igepal CA-630 (all Sigma). Nuclei were then spun down and then resuspend in 25 μL TD (2x reaction buffer),2.5 μL TDE1 (Nextera Tn5 Transposase) and 22.5 μL nuclease-free water, incubated for 30 min at 37°C. DNA was purified with the QIAGEN MinElute PCR Purification Kit (Thermo Fisher Scientific). PCR amplification was performed with the NEBNext High-Fidelity 2x PCR Master Mix (New England Labs) using custom Nextera PCR Primers containing barcodes. Adaptors were removed with AMPure XP beads according to manufacturer's protocol. Libraries were quantified with the Qubit and submitted for sequencing with a HISeq 3000 (Illumina) by the staff at the Deep-sequencing Facility at the Max-Planck-Institute for Immunobiology and Epigenetics. Sequenced samples were trimmed with Trimmomatic (Bolger et al., 2014), mapped using Bowtie2 (Langmead and Salzberg, 2012) and replicate mapped files merged with SAM tools (Li et al., 2009). Coverage files were generated with deepTools. Open chromatin and differentially regulated chromatin was detected with MACS2 (Zhang et al., 2008) with a p value < 1×10^7 and a q value of less than 0.1 and a 4 fold enrichment threshold. Bed files were analyzed with Bedtools (Quinlan and Hall, 2010). ATAC sequencing data are deposited in GEO under the following subseries code: GSE128592.

ChIP sequencing analysis—Fixed cell pellets (1% paraformaldehyde, 10 minutes, RT) were processed for multiplex RELACS (Arrigoni et al., 2018) and sequenced by the staff at the Deep-sequencing Facility at the Max-Planck-Institute for Immunobiology and Epigenetics. Sequenced samples were trimmed with Trimmomatic, mapped using Bowtie2 and replicate mapped files merged with SAM tools. Heatmaps and profile plots were generated and visualized with deepTools. ChIP sequencing data are deposited in GEO under the following subseries code: GSE128593.

QUANTIFICATION AND STATISTICAL ANALYSIS

Comparisons between two groups were performed using unpaired or paired, two-tailed, Student's t test. Comparisons between more than two groups were performed using one-way or two-way ANOVA and Tukey's multiple comparison test. Statistical analysis was performed using Graphpad Prism 7 Software. Statistical significance: * $p < 0.05$; ** $p < 0.005$; *** $p < 0.0005$; **** $p < 0.0001$.

Further details on statistical analysis are listed in the figure legends.

DATA AND SOFTWARE AVAILABILITY

Accession numbers—RNA, ATAC and ChIP sequencing data presented in this manuscript are deposited in GEO under the superseries accession number GSE128594.

Supplementary Material

Refer to Web version on PubMed Central for supplementary material.

ACKNOWLEDGMENTS

We thank P. Allen, C. Hsieh, B. Edelson, E. Oltz, M. Colonna, D.J. Wu, and S. Huang for helpful discussions; Johan Friden for preparing the graphical abstract; Annette Patterson, Andrea Quintana, and Raima Kyle for mouse genotyping; and the Metabolomics and Deep Sequencing Cores at the Max Planck Institute of Immunobiology and Epigenetics for providing expertise for performing and analyzing experiments. This work was supported by grants from the NIH (AI130152 to T.E., AI110481 to E.J.P. and AI091965 and CA158823 to E.L.P.) and the Max Planck Society.

REFERENCES

Afgan E, Baker D, van den Beek M, Blankenberg D, Bouvier D, Cech M, Chilton J, Clements D, Coraor N, Eberhard C, et al. (2016). The Galaxy platform for accessible, reproducible and collaborative biomedical analyses: 2016 update. Nucleic Acids Res. 44 (W1), W3–W10. [PubMed: 27137889]

Agarwal P, Raghavan A, Nandiwada SL, Curtsinger JM, Bohjanen PR, Mueller DL, and Mescher MF (2009). Gene regulation and chromatin remodeling by IL-12 and type I IFN in programming for CD8 T cell effector function and memory. J. Immunol 183, 1695–1704. [PubMed: 19592655]

Allfrey VG, Faulkner R, and Mirsky AE (1964). Acetylation and Methylation of Histones and Their Possible Role in the Regulation of Rna Synthesis. Proc. Natl. Acad. Sci. USA 51, 786–794. [PubMed: 14172992]

Araki Y, Fann M, Wersto R, and Weng NP (2008). Histone acetylation facilitates rapid and robust memory CD8 T cell response through differential expression of effector molecules (eomesodermin and its targets: perforin and granzyme B). J. Immunol 180, 8102–8108. [PubMed: 18523274]

Arrigoni L, Al-Hasani H, Ramírez F, Panzeri I, Ryan DP, Santacruz D, Kress N, Pospisilik JA, Bönisch U, and Manke T (2018). RELACS nuclei barcoding enables high-throughput ChIP-seq. Commun. Biol 1, 214. [PubMed: 30534606]

Balmer ML, Ma EH, Bantug GR, Grählert J, Pfister S, Glatter T, Jauch A, Dimeloe S, Slack E, Dehio P, et al. (2016). Memory CD8(+) T Cells Require Increased Concentrations of Acetate Induced by Stress for Optimal Function. Immunity 44, 1312–1324. [PubMed: 27212436]

Bengsch B, Johnson AL, Kurachi M, Odorizzi PM, Pauken KE, Attanasio J, Stelekati E, McLane LM, Paley MA, Delgoffe GM, and Wherry EJ (2016). Bioenergetic Insufficiencies Due to Metabolic Alterations Regulated by the Inhibitory Receptor PD-1 Are an Early Driver of CD8(+) T Cell Exhaustion. Immunity 45, 358–373. [PubMed: 27496729]

Bolger AM, Lohse M, and Usadel B (2014). Trimmomatic: a flexible trimmer for Illumina sequence data. Bioinformatics 30, 2114–2120. [PubMed: 24695404]

Buck MD, O'Sullivan D, and Pearce EL (2015). T cell metabolism drives immunity. J. Exp. Med 212, 1345–1360. [PubMed: 26261266]

Buck MD, Sowell RT, Kaech SM, and Pearce EL (2017). Metabolic Instruction of Immunity. Cell 169, 570–586. [PubMed: 28475890]

Buenrostro JD, Wu B, Chang HY, and Greenleaf WJ (2015). ATAC-seq: A Method for Assaying Chromatin Accessibility Genome-Wide. Curr. Protoc. Mol. Biol 109, 21.29.1–9.

Bulusu V, Tumanov S, Michalopoulou E, van den Broek NJ, MacKay G, Nixon C, Dhayade S, Schug ZT, Vande Voorde J, Blyth K, et al. (2017). Acetate Recapturing by Nuclear Acetyl-CoA Synthetase 2 Prevents Loss of Histone Acetylation during Oxygen and Serum Limitation. Cell Rep. 18, 647–658. [PubMed: 28099844]

Cham CM, and Gajewski TF (2005). Glucose availability regulates IFN-γamma production and p70S6 kinase activation in CD8+ effector T cells.J. Immunol 174, 4670–4677. [PubMed: 15814691]

Cham CM, Driessens G, O'Keefe JP, and Gajewski TF (2008). Glucose deprivation inhibits multiple key gene expression events and effector functions in CD8+ T cells. Eur. J. Immunol 38, 2438–2450. [PubMed: 18792400]

Chang CH, Curtis JD, Maggi LB Jr., Faubert B, Villarino AV, O'Sullivan D, Huang SC, van der Windt GJ, Blagih J, Qiu J, et al. (2013). Post-transcriptional control of T cell effector function by aerobic glycolysis. Cell 153, 1239–1251. [PubMed: 23746840]

Chang CH, Qiu J, O'Sullivan D, Buck MD, Noguchi T, Curtis JD, Chen Q, Gindin M, Gubin MM, van der Windt GJ, et al. (2015). Metabolic Competition in the Tumor Microenvironment Is a Driver of Cancer Progression. Cell 162, 1229–1241. [PubMed: 26321679]

Comerford SA, Huang Z, Du X, Wang Y, Cai L, Witkiewicz AK, Walters H, Tantawy MN, Fu A, Manning HC, et al. (2014). Acetate dependence of tumors. Cell 159, 1591–1602. [PubMed: 25525877]

Dobin A, Davis CA, Schlesinger F, Drenkow J, Zaleski C, Jha S, Batut P, Chaisson M, and Gingeras TR (2013). STAR: ultrafast universal RNA-seq aligner. Bioinformatics 29, 15–21. [PubMed: 23104886]

Ghoneim HE, Fan Y, Moustaki A, Abdelsamed HA, Dash P, Dogra P, Carter R, Awad W, Neale G, Thomas PG, et al. (2017). De Novo Epigenetic Programs Inhibit PD-1 Blockade-Mediated T Cell Rejuvenation. Cell 170, 142–157.e19. [PubMed: 28648661]

Göttlicher M, Minucci S, Zhu P, Krämer OH, Schimpf A, Giavara S, Sleeman JP, Lo Coco F, Nervi C, Pelicci PG, and Heinzel T (2001). Valproic acid defines a novel class of HDAC inhibitors inducing differentiation of transformed cells. EMBO J. 20, 6969–6978. [PubMed: 11742974]

Halestrap AP, and Wilson MC (2012). The monocarboxylate transporter family–role and regulation. IUBMB Life 64, 109–119. [PubMed: 22162139]

Ho PC, Bihuniak JD, Macintyre AN, Staron M, Liu X, Amezquita R, Tsui YC, Cui G, Micevic G, Perales JC, et al. (2015). Phosphoenolpyruvate Is a Metabolic Checkpoint of Anti-tumor T Cell Responses. Cell 162, 1217–1228. [PubMed: 26321681]

Hosios AM, and Vander Heiden MG (2014). Acetate metabolism in cancer cells. Cancer Metab. 2, 27. [PubMed: 25505945]

Huang W, Sherman BT, and Lempicki RA (2009a). Bioinformatics enrichment tools: paths toward the comprehensive functional analysis of large gene lists. Nucleic Acids Res. 37, 1–13. [PubMed: 19033363]

Huang W, Sherman BT, and Lempicki RA (2009b). Systematic and integrative analysis of large gene lists using DAVID bioinformatics resources. Nat. Protoc 4, 44–57. [PubMed: 19131956]

Jacobs SR, Herman CE, Maciver NJ, Wofford JA, Wieman HL, Hammen JJ, and Rathmell JC (2008). Glucose uptake is limiting in T cell activation and requires CD28-mediated Akt-dependent and independent pathways.J. Immunol 180, 4476–4486. [PubMed: 18354169]

Kendrick SF, O'Boyle G, Mann J, Zeybel M, Palmer J, Jones DE, and Day CP (2010). Acetate, the key modulator of inflammatory responses in acute alcoholic hepatitis. Hepatology 51, 1988–1997. [PubMed: 20232292]

Kirat D, and Kato S (2006). Monocarboxylate transporter 1 (MCT1) mediates transport of short-chain fatty acids in bovine caecum. Exp. Physiol 91, 835–844. [PubMed: 16857719]

Kirat D, Masuoka J, Hayashi H, Iwano H, Yokota H, Taniyama H, and Kato S (2006). Monocarboxylate transporter 1 (MCT1) plays a direct role in short-chain fatty acids absorption in caprine rumen. J. Physiol 576, 635–647. [PubMed: 16901943]

Langmead B, and Salzberg SL (2012). Fast gapped-read alignment with Bowtie 2. Nat. Methods 9, 357–359. [PubMed: 22388286]

Li H, Handsaker B, Wysoker A, Fennell T, Ruan J, Homer N, Marth G, Abecasis G, and Durbin R; 1000 Genome Project Data Processing Subgroup (2009). The Sequence Alignment/Map format and SAMtools. Bioinformatics 25, 2078–2079. [PubMed: 19505943]

Liao Y, Smyth GK, and Shi W (2014). featureCounts: an efficient general purpose program for assigning sequence reads to genomic features. Bioinformatics 30, 923–930. [PubMed: 24227677]

Lin CC, Bradstreet TR, Schwarzkopf EA, Sim J, Carrero JA, Chou C, Cook LE, Egawa T, Taneja R, Murphy TL, et al. (2014). Bhlhe40 controls cytokine production by T cells and is essential for pathogenicity in autoimmune neuroinflammation. Nat. Commun 5, 3551. [PubMed: 24699451]

Love MI, Huber W, and Anders S (2014). Moderated estimation of fold change and dispersion for RNA-seq data with DESeq2. Genome Biol. 15, 550. [PubMed: 25516281]

Lyssiotis CA, and Cantley LC (2014). Acetate fuels the cancer engine. Cell 159, 1492–1494. [PubMed: 25525870]

Ma EH, Bantug G, Griss T, Condotta S, Johnson RM, Samborska B, Mainolfi N, Suri V, Guak H, Balmer ML, et al. (2017). Serine Is an Essential Metabolite for Effector T Cell Expansion. Cell Metab. 25, 345–357. [PubMed: 28111214]

MacIver NJ, Michalek RD, and Rathmell JC (2013). Metabolic regulation of T lymphocytes. Annu. Rev. Immunol 31, 259–283. [PubMed: 23298210]

Mellor AL, and Munn DH (2008). Creating immune privilege: active local suppression that benefits friends, but protects foes. Nat. Rev. Immunol 8, 74–80. [PubMed: 18064049]

Merezhinskaya N, Ogunwuyi SA, Mullick FG, and Fishbein WN (2004). Presence and localization of three lactic acid transporters (MCT1, −2, and −4) in separated human granulocytes, lymphocytes, and monocytes. J. Histochem. Cytochem 52, 1483–1493. [PubMed: 15505343]

Mews P, Donahue G, Drake AM, Luczak V, Abel T, and Berger SL (2017). Acetyl-CoA synthetase regulates histone acetylation and hippocampal memory. Nature 546, 381–386. [PubMed: 28562591]

Michalek RD, and Rathmell JC (2010). The metabolic life and times of a T-cell. Immunol. Rev 236, 190–202. [PubMed: 20636818]

Mockler MB, Conroy MJ, and Lysaght J (2014). Targeting T cell immuno-metabolism for cancer immunotherapy; understanding the impact of the tumor microenvironment. Front. Oncol 4, 107. [PubMed: 24904823]

Nuutinen H, Lindros K, Hekali P, and Salaspuro M (1985). Elevated blood acetate as indicator of fast ethanol elimination in chronic alcoholics. Alcohol 2, 623–626. [PubMed: 4026986]

O'Sullivan D, and Pearce EL (2015). Immunology. Expanding the role of metabolism in T cells. Science 348, 976–977. [PubMed: 26023125]

Patsoukis N, Bardhan K, Chatterjee P, Sari D, Liu B, Bell LN, Karoly ED, Freeman GJ, Petkova V, Seth P, et al. (2015). PD-1 alters T-cell metabolic reprogramming by inhibiting glycolysis and promoting lipolysis and fatty acid oxidation. Nat. Commun 6, 6692. [PubMed: 25809635]

Pauken KE, Sammons MA, Odorizzi PM, Manne S, Godec J, Khan O, Drake AM, Chen Z, Sen DR, Kurachi M, et al. (2016). Epigenetic stability of exhausted T cells limits durability of reinvigoration by PD-1 blockade. Science 354, 1160–1165. [PubMed: 27789795]

Pearce EL, and Pearce EJ (2013). Metabolic pathways in immune cell activation and quiescence. Immunity 38, 633–643. [PubMed: 23601682]

Pearce EL, Poffenberger MC, Chang CH, and Jones RG (2013). Fueling immunity: insights into metabolism and lymphocyte function. Science 342, 1242454. [PubMed: 24115444]

Peng M, Yin N, Chhangawala S, Xu K, Leslie CS, and Li MO (2016). Aerobic glycolysis promotes T helper 1 cell differentiation through an epigenetic mechanism. Science 354, 481–484. [PubMed: 27708054]

Puleston DJ, Villa M, and Pearce EL (2017). Ancillary Activity: Beyond Core Metabolism in Immune Cells. Cell Metab. 26, 131–141. [PubMed: 28683280]

Quinlan AR, and Hall IM (2010). BEDTools: a flexible suite of utilities for comparing genomic features. Bioinformatics 26, 841–842. [PubMed: 20110278]

Rae C, Fekete AD, Kashem MA, Nasrallah FA, and Bröer S (2012). Metabolism, compartmentation, transport and production of acetate in the cortical brain tissue slice. Neurochem. Res 37, 2541–2553. [PubMed: 22851350]

Ramírez F, Ryan DP, Grüning B, Bhardwaj V, Kilpert F, Richter AS, Heyne S, Dündar F, and Manke T (2016). deepTools2: a next generation web server for deep-sequencing data analysis. Nucleic Acids Res. 44 (W1), W160–W165. [PubMed: 27079975]

Renner K, Singer K, Koehl GE, Geissler EK, Peter K, Siska PJ, and Kreutz M (2017). Metabolic Hallmarks of Tumor and Immune Cells in the Tumor Microenvironment. Front. Immunol 8, 248. [PubMed: 28337200]

Saucillo DC, Gerriets VA, Sheng J, Rathmell JC, and Maciver NJ (2014). Leptin metabolically licenses T cells for activation to link nutrition and immunity. J. Immunol 192, 136–144. [PubMed: 24273001]

Schug ZT, Peck B, Jones DT, Zhang Q, Grosskurth S, Alam IS, Goodwin LM, Smethurst E, Mason S, Blyth K, et al. (2015). Acetyl-CoA synthetase 2 promotes acetate utilization and maintains cancer cell growth under metabolic stress. Cancer Cell 27, 57–71. [PubMed: 25584894]

Siska PJ, Beckermann KE, Mason FM, Andrejeva G, Greenplate AR, Sendor AB, Chiang YJ, Corona AL, Gemta LF, Vincent BG, et al. (2017). Mitochondrial dysregulation and glycolytic insufficiency functionally impair CD8 T cells infiltrating human renal cell carcinoma. JCI Insight 2, 93411. [PubMed: 28614802]

Szabo SJ, Kim ST, Costa GL, Zhang X, Fathman CG, and Glimcher LH (2000). A novel transcription factor, T-bet, directs Th1 lineage commitment. Cell 100, 655–669. [PubMed: 10761931]

Trompette A, Gollwitzer ES, Pattaroni C, Lopez-Mejia IC, Riva E, Pernot J, Ubags N, Fajas L, Nicod LP, and Marsland BJ (2018). Dietary Fiber Confers Protection against Flu by Shaping Ly6c(−) Patrolling Monocyte Hematopoiesis and CD8(+) T Cell Metabolism. Immunity 48, 992–1005.e8. [PubMed: 29768180]

Verdin E, and Ott M (2015). 50years ofproteinacetylation:fromgeneregulation to epigenetics, metabolism and beyond. Nat. Rev. Mol. Cell Biol. 16, 258–264. [PubMed: 25549891]

Watkins PA, Maiguel D, Jia Z, and Pevsner J (2007). Evidence for 26 distinct acyl-coenzyme A synthetase genes in the human genome. J. Lipid Res. 48, 2736–2750. [PubMed: 17762044]

Wedemeyer H, He XS, Nascimbeni M, Davis AR, Greenberg HB, Hoof-nagle JH, Liang TJ, Alter H, and Rehermann B (2002). Impaired effector function of hepatitis C virus-specific CD8+ T cells in chronic hepatitis C virus infection. J. Immunol 169, 3447–3458. [PubMed: 12218168]

Zhang Y, Liu T, Meyer CA, Eeckhoute J, Johnson DS, Bernstein BE, Nusbaum C, Myers RM, Brown M, Li W, and Liu XS (2008). Model-based analysis of ChIP-Seq (MACS). Genome Biol. 9, R137. [PubMed: 18798982]

Highlights

- Acetate restores IFN-γ in TILs and T cells under prolonged glucose-restriction
- Acetate promotes histone acetylation and chromatin accessibility in T cells
- ACSS expression contributes to optimal effector T cell function during cancer
- Acetate Promotes T Cell Effector Function during Glucose Restriction

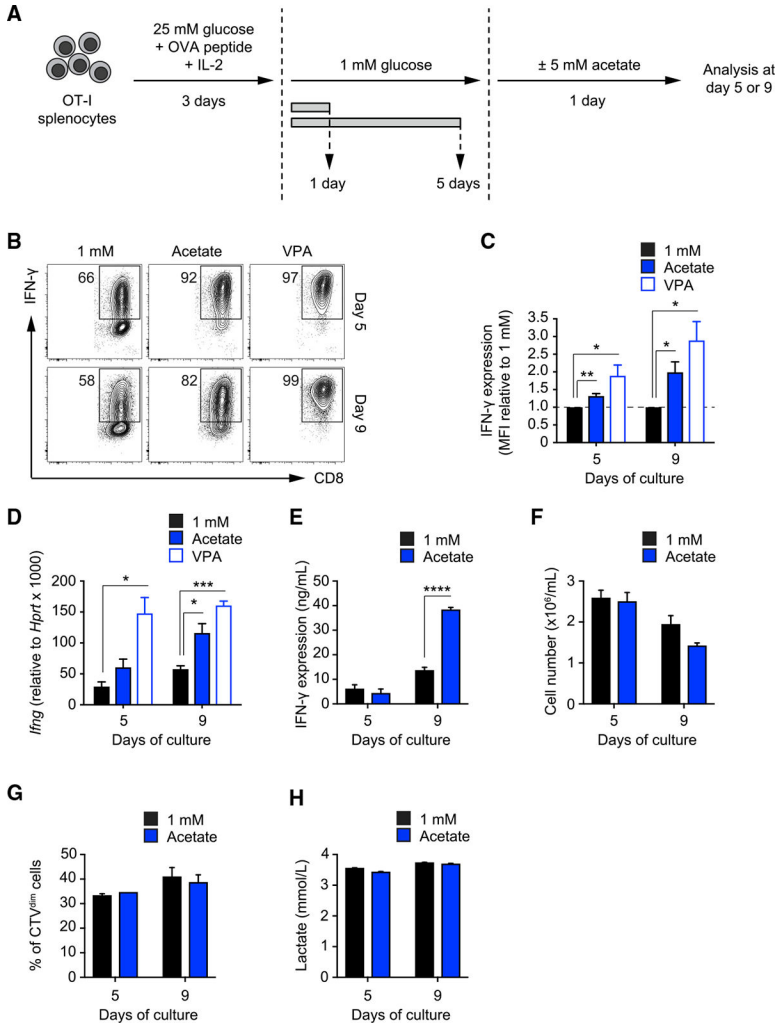

Figure 1. Supplemental Acetate Promotes IFN-γ Production in T Cells under Chronic Glucose Restriction

(A) *In vitro* culture system. Splenic naive OT-I CD8$^+$ T cells were activated with SIINFEKL peptide and IL-2 and maintained for 3 days in medium containing 25 mM glucose. Then T cells were transferred to medium containing 1 mM glucose for an additional 1 or 5 days. 1 day prior to analysis, T cells were treated with or without 5 mM acetate. Analysis was performed on days 5 and 9.

(B) FACS analysis of IFN-γ production by T cells cultured as described in (A). Numbers show percentages of IFN-γ$^+$ cells. VPA, valproic acid. FACS plots are representative of n = 4 independent experiments.

(C) Quantification of IFN-γ production as mean fluorescent intensity (MFI) of the CD8$^+$ population. Values were normalized to the 1 mM condition. Mean ± SEM, Student's t test, n = 4 independent experiments.

(D) Real-time PCR of *Ifng* mRNA in cells cultured as described in (A). Values were normalized to *Hprt*. Mean ± SEM, Student's t test, n = 3 independent experiments.

(E) ELISA quantification of IFN-γ production by T cells cultured as described in (A) upon restimulation of 10^6 cells with PMA-ionomycin for 4 h. Mean ± SEM, Student's t test, n = 3 independent experiments.

(F) Number of live cells harvested after 24 h of culture under the indicated conditions after seeding 10^6 cells/mL. Mean ± SEM, n = 2 independent experiments.

(G) Analysis of cell proliferation using CellTrace Violet dye. The graph shows the fraction of cells diluting the dye over 24 h of culture under the indicated conditions. Mean ± SEM, n = 2 independent experiments.

(H) Quantification of lactate production as a measure of aerobic glycolysis in the medium of cells cultured for 24 h under the indicated conditions. Mean ± SEM, n = 2 independent experiments.

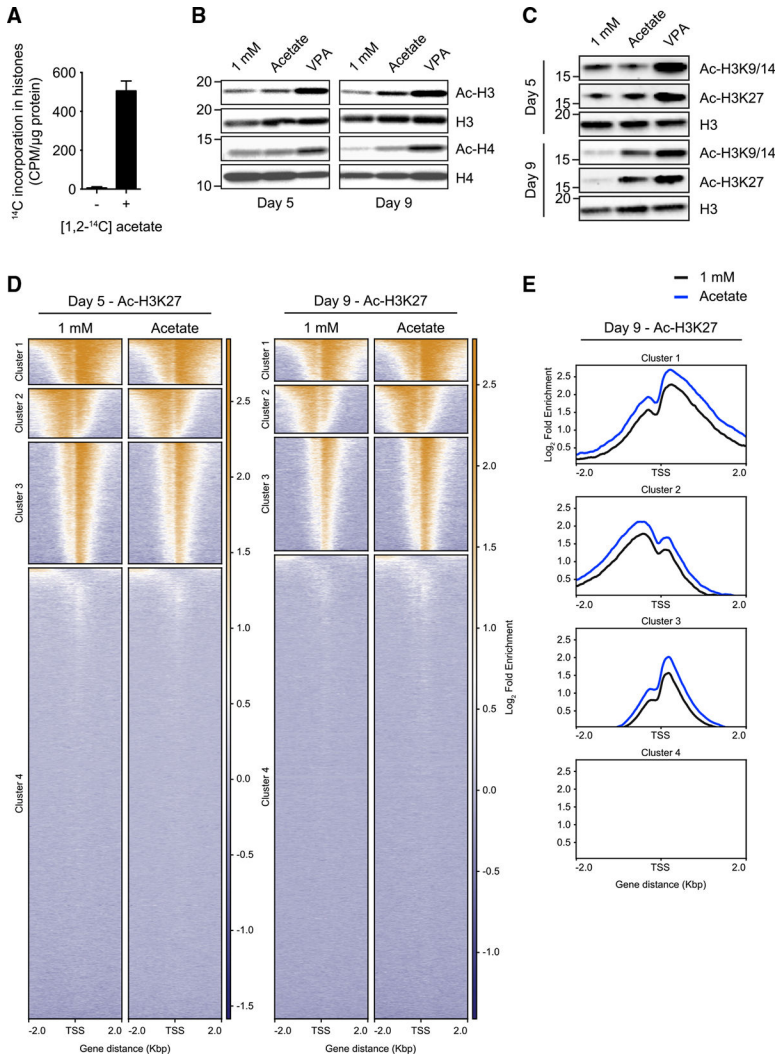

Figure 2. Acetate Is Incorporated into His-tones and Enhances Histone Acetylation in Glucose-Restricted T Cells

(A) Quantification of [1,2-^{14}C] acetate-derived ^{14}C incorporation in histones extracted from T cells cultured in 10 mM glucose medium. Mean ± SEM; n = 2 independent experiments.

(B) Western blot analysis of global histone acetylation (acetylated histones H3 and H4) in T cells treated as described in Figure 1A. Data are representative of n = 2 independent experiments.

(C) Western blot analysis of H3K9–14 and H3K27 acetylation in T cells treated as described in Figure 1A. Data are representative of n = 2 independent experiments.

(D) Genome-wide chromatin immunoprecipitation sequencing (ChIP-seq) analysis of acetylation of H3K27 in T cells treated as described in Figure 1A. On the y axis, every line represents the acetylation profile of a specific gene. Genes were clustered according to the H3K27 acetylation profile pattern. Reported on the x axis is the distance from the transcription start site (TSS) of every gene. The bars on the side of each graph represent the fold enrichment, following a color scheme (orange, high enrichment; blue, low enrichment). n = 2 biological replicates.

(E) Global representation of the data shown in (D) (day 9) as an enrichment profile. Culture conditions are reported in the color legend. On the y axis, the fold enrichment is shown. Reported on the x axis is the distance from the TSS.

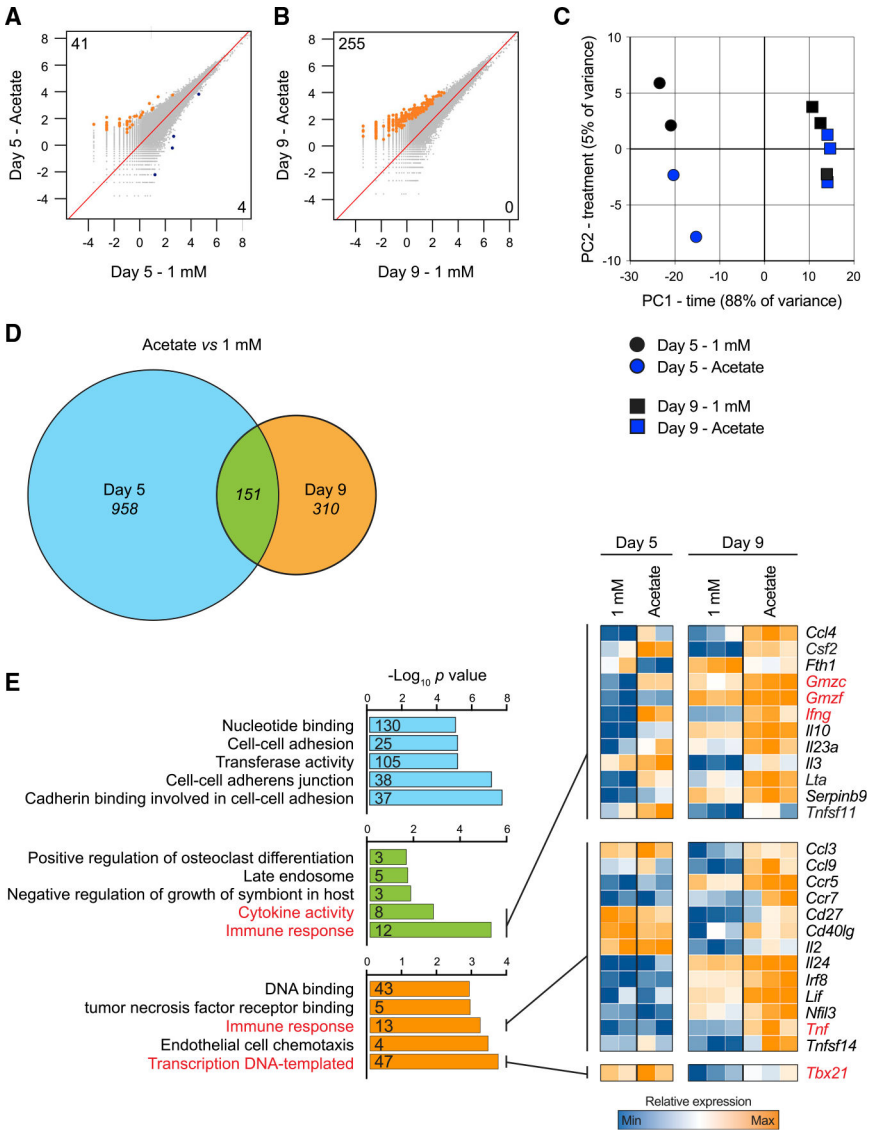

Figure 3. Acetate Promotes Chromatin Accessibility in Glucose-Restricted T Cells

(A and B) ATAC-seq analysis of genome-wide chromatin accessibility in T cells cultured as described in Figure 1A. (A) shows comparisons on day 5 post-activation, whereas (B) shows comparisons on day 9 post-activation. Numbers indicate chromatin regions with significantly enhanced (orange, top left corner value) or significantly reduced (blue, bottom right corner value) accessibility. The term of comparison for each analysis is the 1 mM condition, either on day 5 (A) or on day 9

(B). n = 3 biological replicates. Values on the axis show $\log_2$ reads per million (RPM).

(C) Principal-component analysis (PCA) of RNA-seq data obtained from cells cultured as in Figure 1A and restimulated with PMA-ionomycin for 4 h. n = 2–3 biological replicates.

(D) Venn diagram showing the differentially expressed genes (DEGs) on day 5, on day 9, and at both time points in cells cultured in 1 mM glucose versus cells exposed to acetate 1 day prior to analysis. DEGs were filtered on adjusted p values lower than 0.1 and fold changes greater than 30%. n = 2–3 biological replicates.

(E) Gene ontology analysis of the DEGs identified from comparison of cells cultured in 1 mM glucose versus cell exposed to acetate. The color-coding refers to (D). The heatmaps show a selection of genes belonging to the identified gene ontology terms. Gene ontology terms and genes of particular interest are highlighted in red. Numbers included in the bars indicate the number of DEGs belonging to each gene ontology term. The top 5 gene ontology terms are shown. Blue, low expression; orange, high expression.

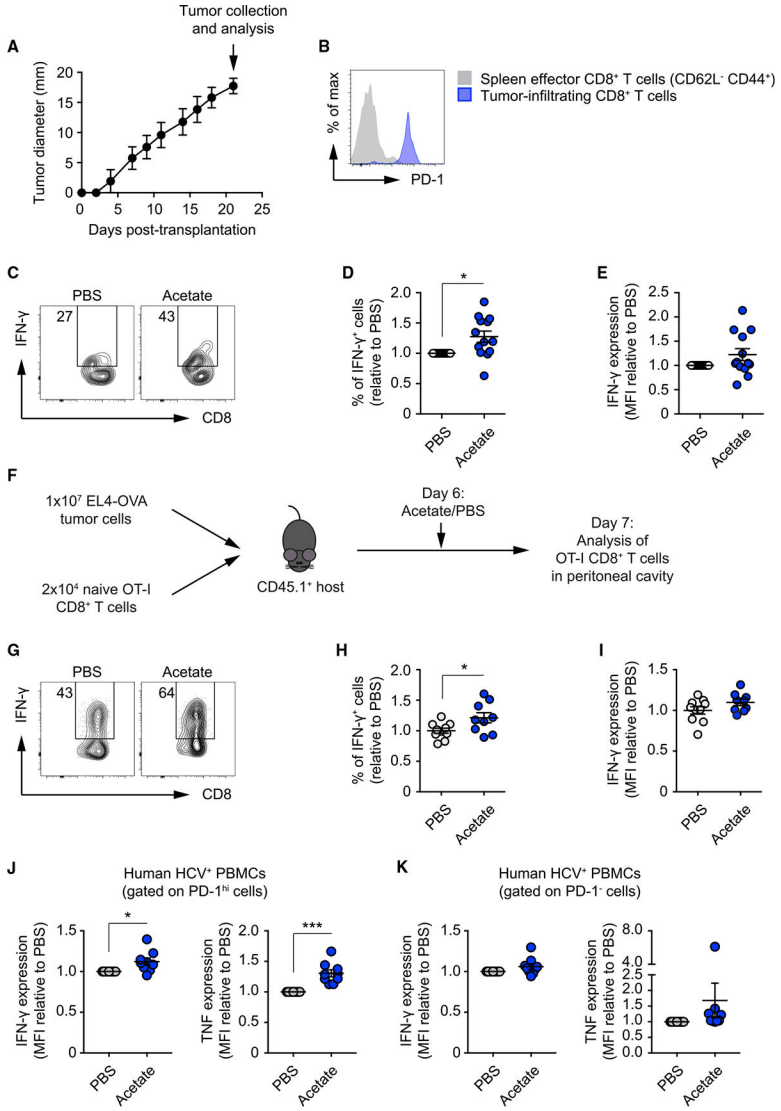

Figure 4. Supplemental Acetate Increases IFN-γ Production by TILs

(A) Growth curve of B16 melanoma tumors subcutaneously implanted in C57BL/6 recipient mice. Data show the average of two perpendicular diameters ± range. 14 mice were monitored.

(B) FACS analysis of PD-1 expression in splenic $CD62L^{-}CD44^{+}$ $CD8^{+}$ T effector cells and $CD8^{+}$ tumor-infiltrating lymphocytes (TILs) isolated on day 21 post-tumor implant. Data are representative of 3 independent experiments.

(C) FACS analysis of IFN-γ production by TILs isolated 21 days post-tumor implantation and treated overnight with either PBS or 5 mM acetate. Numbers show percentages of IFN-γ^{+} cells. FACS plots are representative of 3 independent experiments.

(D and E) Quantification of percentages of IFN-γ^{+} cells (D) and MFI of IFN-γ staining (E) as in (C). Values are normalized to the PBS condition. Mean ± SEM, paired Student's t test; data were pooled from 3 independent experiments.

(F) 1×10^{6} EL4-OVA lymphoma cells were injected intraperitoneally, and 2×10^{4} naive OT-I $CD8^{+}$ T cells were injected intravenously into $CD45.1^{+}$ C57BL/6 recipient mice. 6 days

later, mice received a single intraperitoneal bolus of 500 mg/kg acetate or PBS. Analysis was performed 1 day later.

(G) FACS analysis of IFN-γ production by OT-I $CD8^+$ T cells isolated from the peritoneal cavity of recipient mice. Numbers show percentages of IFN-γ^+ cells. FACS plots are representative of 2 independent experiments.

(H and I) Quantification of percentages of IFN-γ^+ cells (H) and MFI of IFN-γ staining (I) as in (G). Values are normalized to the PBS condition. Mean ± SEM, Student's t test; data were pooled from 2 independent experiments.

(J and K) FACS analysis of IFN-γ (J) and TNF (K) production by PBMCs isolated from the blood of chronically infected HCV patients, treated overnight with either PBS or 5 mM acetate. Data show MFI of IFN-γ and TNF staining. Values are normalized to the PBS counterparts. Mean ± SEM, paired Student's t test; data from 9 donors.

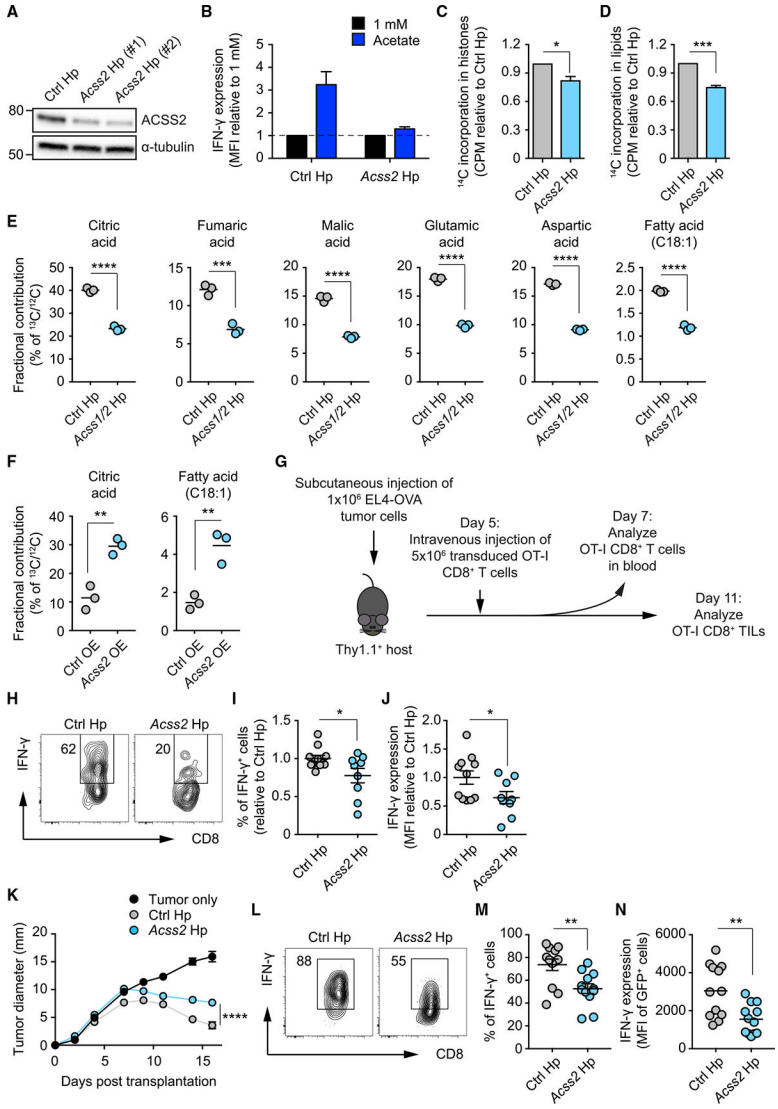

Figure 5. Cell-Intrinsic ACSS2 Expression Contributes to Optimal Effector T Cell Function and Anti-tumor Immunity *In Vivo*

(A) Western blot analysis of ACSS2 in T cells transduced with either control (Ctrl) luciferase shRNA or *Acss2* shRNA. Data are representative of 2 independent experiments.

(B) FACS analysis of IFN-γ MFI in T cells cultured in 1 mM glucose, transduced with Ctrl shRNA or *Acss2* shRNA, and treated with or without acetate. Values were normalized to the 1 mM glucose condition. Mean ± SEM, n = 2 independent experiments.

(C and D) Quantification of [1,2-^{14}C] acetate-derived ^{14}C incorporation in histones (C) and lipids (D) extracted from T cells cultured in 10 mM glucose medium. Values are normalized to Ctrl shRNA. Mean ± SEM, Student's t test; n = 3 independent experiments.

(E and F) Gas chromatography-mass spectrometry (GC-MS) analysis of ^{13}C-acetate-derived ^{13}C fractional contribution in metabolites extracted from T cells transduced with Ctrl shRNA or *Acss1/2* shRNA (E), Ctrl empty vector (Ctrl overexpression [OE]), or *Acss2* enforced expressor (*Acss2*-OE) (F). Mean, Student's t test; n = 3 biological replicates.

(G) 1×10^6 EL4-OVA lymphoma cells were injected subcutaneously into Thy1.1$^+$ C57BL/6 recipient mice. 5 days later, mice were intravenously administered 5×10^6 OT-I CD8$^+$ T cells transduced with Ctrl shRNA or *Acss2* shRNA. Analysis of blood CD8$^+$ T cells was performed 2 days later.

(H) FACS analysis of IFN-γ production by OT-I CD8$^+$ T cells isolated from the blood of recipient mice. Numbers show percentages of IFN-γ$^+$ cells. FACS plots are representative of 2 independent experiments.

(I and J) Quantification of percentage of IFN-γ$^+$ cells (I) and MFI of IFN-γ staining (J) as in (H). Values are normalized to the Ctrl shRNA condition. Mean ± SEM, Student's t test; data were pooled from 2 independent experiments.

(K) Growth curve of EL4-OVA lymphoma tumors, subcutaneously implanted in Thy1.1$^+$ C57BL/6 recipient mice, upon administration on day 5 post-implant of PBS or OT-I CD8$^+$ T cells transduced with either Ctrl shRNA or *Acss2* shRNA. Data show the average of two perpendicular diameters ± SEM; two-way ANOVA with Tukey's multiple comparisons test; n = 4 mice/group, representative of 2 independent experiments.

(L) FACS analysis of IFN-γ production by OT-I CD8$^+$ TILs isolated from tumors of recipient mice. Numbers show percentages of IFN-γ$^+$ cells of the shRNA-transduced GFP$^+$ population. FACS plots are representative of 3 independent experiments.

(M and N) Quantification of percentages of IFN-γ$^+$ cells (M) and MFI of IFN-γ staining (N) as in (L). Mean ± SEM, Student's t test; data from 3 experiments.

KEY RESOURCES TABLE

REAGENT or RESOURCE	SOURCE	IDENTIFIER
Antibodies		
Anti-mouse CD8α	Biolegend	Clone 53–6.7
Anti-mouse CD44	Biolegend	Clone IM7
Anti-mouse CD45.1	Biolegend	Clone A20
Anti-mouse CD45.2	Biolegend	Clone 104
Anti-mouse PD-1	Invitrogen	Clone J43
Anti-mouse CD25	Biolegend	Clone 3C7
Anti-mouse CD69	Biolegend	Clone H1.2F3
Anti-mouse CD62L	Biolegend	Clone MEL-14
Anti-mouse CD71	Biolegend	Clone RI7217
Anti-mouse Granzyme B	eBioscience	Clone NGZB
Anti-mouse IFN-γ	Biolegend	Clone XMG1.2
Anti-GFP	Biolegend	Clone FM264G
Anti-mouse α Tubulin	Cell Signaling	Clone 11H10
Anti-mouse ACSS2	Thermo Scientific	Cat. PA5–26612
Anti-mouse MCT-4	Santa Cruz	Clone H-90 sc-50329
Anti-mouse MCT-1	Santa Cruz	Clone T-19 sc-14917
Anti-mouse H3	Cell Signaling	Cat. 9715
Anti-mouse H4	Cell Signaling	Cat. 13919
Anti-mouse acetylated H3	Millipore	Cat. 06–599
Anti-mouse acetylated H4	Millipore	Cat. 06–866
Anti-mouse acetylated H3K9/14	Diagenode	Cat. C15410200
Anti-mouse acetylated H3K27	Diagenode	Cat. C15410196
Bacterial and Virus Strains		
Ctrl hairpin	Open Biosystems	MSCV-LTRmiR30-PIG (LMP) Addgene plasmid #24071
Acss1 hairpin (same backbone as Ctrl hairpin and Acss1 sequence)	Open Biosystems	MSCV-LTRmiR30-PIG (LMP) Addgene plasmid #24071
Acss2 hairpin (same backbone as Ctrl hairpin and Acss2 sequence)	Open Biosystems	MSCV-LTRmiR30-PIG (LMP) Addgene plasmid #24071
Ctrl MigR1	Gift from Steve Reiner	MIGR1 plasmid #27490
Acss2 MigR1	Dharmacon	MGC Mouse Acss2 cDNA(Clone ID: 6515568)
Biological Samples		
HCV-infected blood	Uniklinik Freiburg (Dr. Bertram Bengsch)	NA
Chemicals, Peptides, and Recombinant Proteins		
SIINFEKL peptide	New England Peptide	Cat. BP10–915
FBS	GIBCO	Lot. 1640960
Recombinant human IL-2	Peprotech	Cat. 200–02
Sodium Acetate Trihydrate	Sigma	Cat. 71188
Valproic Acid Sodium Salt	Sigma	Cat. P4543
Type IA Collagenase	Sigma	SCR103

REAGENT or RESOURCE	SOURCE	IDENTIFIER
DNase I	Sigma	Cat. 11284932001
[1,2-^{14}C] Acetate	Perkin Elmer	Cat. NEC084A001MC
Critical Commercial Assays		
Anti-mouse IFN-γ ELISA kit	RND Systems	Cat. DY485
Deposited Data		
RNA-seq	This manuscript	GSE128591
ATAC-seq	This manuscript	GSE128592
ChIP-seq	This manuscript	GSE128593
Experimental Models: Cell Lines		
B16 melanoma tumor cell line	Dr. Marco Colonna	NA
EL4-OVA	ATCC	CRL-2113
Experimental Models: Organisms/Strains		
OT-I transgenic mice	Jackson Labs.	#003831
CD45.1 C57B176J mice	Jackson Labs.	#002014
Thy1.1^{+} C57BIV6Jmice	Jackson Labs.	#000406
C57B176J mice	Jackson Labs.	#000664
Oligonucleotides		
Taqman primers: Ifng	Applied Biosystems	MmO1168134_m1
Taqman primers: Hprt	Applied Biosystems	Mm03024075_m1
Recombinant DNA		
Acss1 hairpin Black: 5′ miR30 context Blue: Acss1 sense sequence Green: Loop Red: Acss1 antisense sequence Black: 3′ miR30 context	Sigma	TGCTGTTGACAGTGAGCGCCCCAAGGGACTC GTTCATACATAGTGAAGCCACAGATGTATGTA TGAACGAGTCCCTTGGGTTGCCTACTGCCTCGGA
Acss2 hairpin Black: 5′ miR30 context Blue: Acss2 sense sequence Green: Loop Red: Acss2 antisense sequence Black: 3′ miR30 context	Sigma	TGCTGTTGACAGTGAGCGACACCGGGTAGTA GGTTCCCAATAGTGAAGCCACAGATGTATTG GGAACCTACTACCCGGTGGTGCCTACTGCC TCGGA
Software and Algorithms		
Galaxy platform	Afgan et al., 2016	NA
Deeptools	Ramírez et al., 2016	NA
STAR	Dobin et al., 2013	NA
FeatureCounts	Liao et al., 2014	NA
DESeq2	Love et al., 2014	NA
Morpheus	Broad Institute	NA
DAVID	Huang et al., 2009b	NA
Trimmomatic	Bolger et al., 2014	NA
Bowtie2	Langmead and Salzberg, 2012	NA
SAM tools	Li et al., 2009	NA
MACS2	Zhang et al., 2008	NA
Bedtools	Quinlan and Hall, 2010	NA